Ag/Cu(111) structure revisited through an extended mechanism for stress relaxation

Isabelle Meunier, Guy Tréglia, Jean-Marc Gay, and Bernard Aufray
CRMC2, Centre National de la Recherche Scientifique, Campus de Luminy, Case 913, 13288 Marseille Cedex 9, France*

Bernard Legrand
SRMP-DECM, CEA Saclay, 91191 Gif-sur-Yvette Cedex, France
(Received 27 October 1998)

The Ag/Cu(111) system can be considered as a model one concerning the atomic structure of one monolayer deposited on a substrate in the case of strong size mismatch. Thus, it has been the subject of many experimental [Auger electron spectroscopy, low-energy electron diffraction and scanning tunneling microscopy (STM)] and theoretical studies, in particular within *N*-body potentials. Although most results agreed both with the existence of an $n\times n$ superstructure accommodating the size mismatch and with a strong corrugation of the Ag adlayer, the morphologies—derived from STM on the one hand and numerical simulations on the other hand—were not found to be consistent. Here we revisit the previous theoretical study, taking into account different additional mechanisms (Ag and Cu vacancy formation, partial dislocation loop) to relax the interfacial stress. As a result, we obtain that the most efficient relaxation mechanism is the formation of partial dislocation loops in the first Cu substrate layer, requiring the formation of four or five Cu vacancies per unit cell in this plane. This leads to a strong damping of the corrugation in the Cu underlayers, and a perfect agreement is reached between observed and calculated surface morphology. [S0163-1829(99)14915-4]

I. INTRODUCTION

The knowledge of the atomic structure of a monolayer deposited on a substrate is very important for fundamental and technological reasons. This explains the large quantity of works on this subject. In particular the influence of size mismatch between the deposit and the substrate has been largely investigated.[1–7] From this point of view, the Ag/Cu (111) system can be considered as representative of the case: a large deposit atom and small substrate atom for two species which are almost completely immiscible in the bulk. Thus, it has been the subject of many experimental[8–20] and theoretical[21–23] studies. The first experiments were performed by low-energy electron diffraction (LEED):[10] they put into evidence the existence of a $(10\pm1)\times(10\pm1)$ superstructure suited to the coincidence mesh corresponding to the size mismatch between Ag and Cu (about 13%). The existence of such a superstructure was confirmed by theoretical calculations performed using quenched molecular dynamics (QMD) simulations, based on an interatomic potential derived from electronic structure in the tight-binding approximation (TB-QMD).[22] In addition, a very large corrugation was predicted both for the Ag adsorbate layer and, more surprisingly, for the first layers of the Cu substrate. It was found that this corrugation is damped only beyond about ten layers.

In order to test these surprising theoretical results, experiments were proposed coupling scanning tunneling microscopy (STM) and surface x-ray diffraction (SXRD).[20] Concerning the periodicity, both types of experiments essentially confirm the LEED conclusions, namely a $n\times n$ superstructure with $9\leqslant n\leqslant 10$ (more precisely, SXRD gives $n=9.43$). Conversely, the morphology of the Ag surface plane displayed by the STM image differs somewhat from the calculated one, as can be seen in Figs. 1(a) and 1(b). In particular the main pattern of the STM image is the presence of deep triangular-shaped regions, edged by either four or five atoms with one or three protruding atoms in the center [Fig. 1(b)]. Conversely the previous TB-QMD calculation only exhibits rounded uniform hollowed regions [Fig. 1(a)].[22] Let us mention that more isotropic shapes (referred to as Moiré structures), similar to those resulting from TB-QMD calculation, have also been observed previously by STM.[17] In fact, more exhaustive STM studies[19] reveal that both structures (triangles and Moiré) can be observed as a function of temperature.

In this paper we show that such triangular-shaped regions can be obtained theoretically, by taking under consideration in the TB-QMD simulation some additional possibilities to relax the interfacial stress. This involves the formation of Ag vacancies in the surface plane, Cu vacancies, and partial dislocation loops in the first underlayer. It is obvious that such phenomena could be hardly observed during realistic times of molecular dynamics simulation. Thus we have to introduce them at the beginning of the simulation. This allows us to compare the energy of the various configurations and to decide which is the most stable one, at least at $T=0$ K. In return, the determination of the atomic mechanism leading to the optimized configuration is clearly beyond the scope of the present work.

The paper is organized as follows. A survey of the model is presented in Sec. II. Then we apply it for the study of the deposit of one Ag monolayer on the Cu(111) substrate, in order to determine the structure which minimizes the adsorption energy (Sec. III). A detailed analysis of this structure and a comparison with the experimental data are proposed in Sec. IV before giving some perspectives (Sec. V).

II. MODEL

As mentioned above, we have to compare structures which differ both by the periodicity and pattern of the unit cell. This requires dealing with different numbers of Ag and Cu atoms in these cells. To this aim, we have to define a pertinent energetic criterion. Such a criterion is the adsorption energy per Ag atom, written in the following way:

$$E_{\mathrm{ads}}^{\mathrm{Ag}_n}=\frac{E_{\mathrm{tot}}(\mathrm{Ag}_n/\mathrm{Cu}_{N-n_v})+n_vE_{\mathrm{coh}}(Cu)-E_{\mathrm{tot}}(\mathrm{Cu}_N)-nE_{\mathrm{free}}(\mathrm{Ag})}{n}, \tag{1}$$

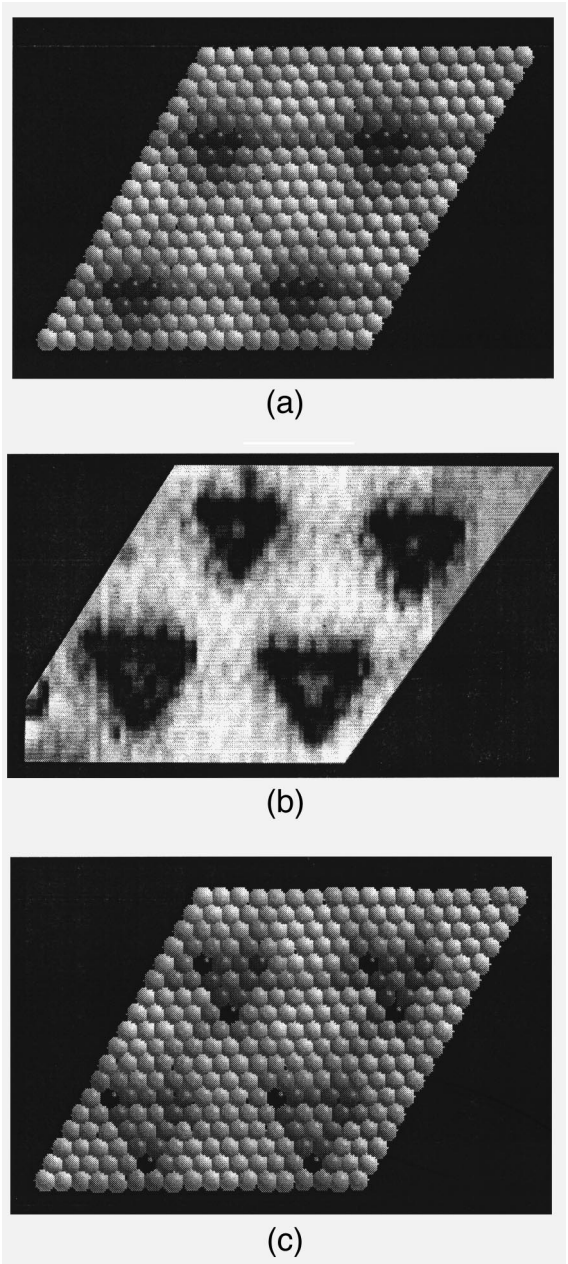

FIG. 1. Ag/Cu microstructure viewed from above. The grey scale has been chosen such that the black (white) dots are associated with the deepest (highest) elevation. The theoretical results are shown in (a) before the introduction of vacancies and in (c) after creation of two domains with respectively four and five vacancies per unit cell. The extreme elevations are $h_{\min}=-0.33$ Å and $h_{\max}=+0.75$ Å. In (b) we recall the experimental STM image (Ref. 20).

where $E_{\mathrm{tot}}(\mathrm{Cu}_N)$ is the total energy of the substrate with N atoms and a (111) surface, $E_{\mathrm{free}}(\mathrm{Ag})$ the energy of an isolated Ag atom (taken as the energy origin), and finally $E_{\mathrm{tot}}(\mathrm{Ag}_n/\mathrm{Cu}_{N-n_v})$ is the total energy of the system, including the Cu substrate with $(N-n_v)$ atoms and the adsorbed layer containing n Ag atoms per unit cell. In this expression, we take into account the possibility to create n_v Cu vacancies in the first substrate layer to minimize the adsorption energy. As for the vacancy formation energy in the bulk, the n_v Cu atoms, which have been taken off, are assumed to be replaced at the Cu chemical potential, i.e., the Cu cohesive energy E_{coh} (Cu). It is worth noting that this grand canonical formalism does not supply any information on the atomic mechanism for the formation of these vacancies, and that it would not apply to eventual intermediate states, such as the integration of the removed Cu atoms in the Ag adsorbate plane. In practice, this means that these Cu atoms are replaced at some pure Cu kinks in step edges. The optimal structure will then be the one which minimizes the adsorption energy [Eq. (1)].

The energetic model is derived in the framework of the tight-binding approximation. More precisely, we write the energy of an atom at site i as the sum of a band contribution, in the form of the square root of the second moment of the local electronic density of states, and a repulsive term of the Born-Mayer type:[24]

$$E_i=E_{\mathrm{band}}^i+E_{\mathrm{rep}}^i, \tag{2}$$

$$E_{\mathrm{band}}^i=-\left\{\sum_{j,r_{ij}<r_c}\xi_{IJ}^2\exp\left[-2q_{IJ}\left(\frac{r_{ij}}{r_0^{IJ}}-1\right)\right]\right\}^{1/2}, \tag{3}$$

$$E_{\mathrm{rep}}^i=\sum_{j,r_{ij}<r_c}A_{IJ}\exp\left[-p_{IJ}\left(\frac{r_{ij}}{r_0^{IJ}}-1\right)\right], \tag{4}$$

where r_{ij} is the distance between atoms at sites i and j, respectively occupied by the I and J chemical species: I,J = Ag or Cu; r_c is the cutoff of the interaction (here beyond second neighbors); and r_0^{II} is the first-neighbor distance in the metal I [$r_0^{IJ}=(r_0^{II}+r_0^{JJ})/2$].

Therefore, the energy depends on three sets of four parameters ξ_{IJ}, A_{IJ}, p_{IJ}, and q_{IJ}, which characterize, respectively, the Ag-Ag, Cu-Cu, and Ag-Cu interactions. The values of these parameters are the same as in the previous tight-binding study.[22] They have been determined for homoatomic interactions (Ag-Ag and Cu-Cu) by fitting the experimental values of the cohesive energy, lattice parameter, and differ-

ent elastic constants. The mixed interactions (Ag-Cu) are determined to reproduce the essential feature of the Ag-Cu phase diagram, namely, the existence of a miscibility gap. This is achieved by fitting the solution energies of both Ag in Cu (-0.38 eV) and Cu in Ag (-0.28 eV).[25]

It is well known that the surface energy of each pure metal is underestimated within this kind of N-body potential, as it is the case for other related methods (embedded-atom method (EAM),[26] effective medium theory (EMT),[27] Finnis-Sinclair potentials,[28] glue model,[29] etc.). However their difference from one element to the other is fortunately well reproduced in the case of Ag and Cu, which is an essential requirement in surface alloys and alloy surfaces studies.[30]

Then the optimized structures are obtained by means of a quenched molecular dynamics algorithm.[31] The atoms are displaced following the interatomic forces F_i calculated as

$$\vec{F}_i = -\frac{dE_{\mathrm{tot}}}{d\vec{r}_i}. \tag{5}$$

The quenching procedure is performed by cancelling the velocity $\vec{v}_i$ of atom i when the product $\vec{F}_i \cdot \vec{v}_i$ becomes negative.[31] This drives the system toward a minimum of energy at T=0 K.

III. OPTIMIZED STRUCTURE OF ONE AG MONOLAYER ON CU(111)

A. Survey of the previous theoretical study

Let us briefly summarize the previous study performed on the Ag/Cu(111) system.[22] The first step was to determine the periodicity of the superstructure at the completion, the latter being defined as the critical coverage beyond which an additional Ag adatom should be located in the second adlayer. This was performed by placing an $(n-1)\times(n-1)$ Ag layer on an $n\times n$ Cu(111) substrate in order to determine the value of n which minimizes the adsorption energy per Ag atom. In fact, what was found was that this energy presents a very smooth minimum in the range $9 \leqslant n \leqslant 11$. This value is close to the value n^* that could be predicted from the simple geometrical criterion of a uniform distribution of the size mismatch all along the close-packed rows, namely,

$$n^* = \frac{1}{1-\dfrac{r^0_{\mathrm{Cu}}}{r^0_{\mathrm{Ag}}}} = 8.76 \tag{6}$$

with $r^0_{\mathrm{Cu}} = 1.28$ Å and $r^0_{\mathrm{Ag}} = 1.445$ Å.

Nevertheless, it is worth pointing out that, even though this simple criterion was apparently satisfied, the distribution of the Ag atoms (and that of the underlying Cu ones) was far from being uniform. Indeed a very strong corrugation occurred, which could be quantified for each plane parallel to the surface as given by the maximum amplitude of elevation between the lowest and highest atoms of this plane. The corresponding corrugation of the first atomic planes was very pronounced, extending into the substrate up to the tenth Cu layer. The Ag adlayer presented a corrugation of about 0.9 Å, whereas a maximum value of 1.2 Å was observed on the first substrate plane (see the curves for $n_v = 0$ in Fig. 2).

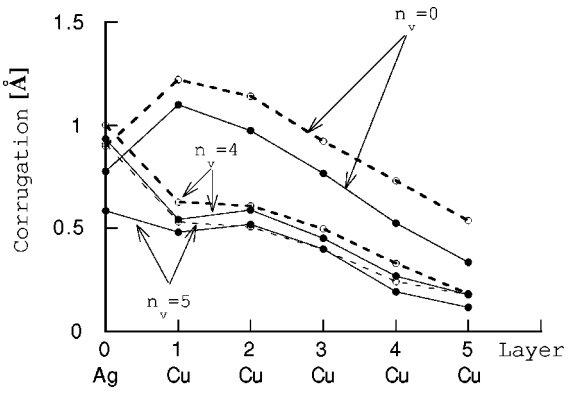

FIG. 2. Corrugation profile (in Å) associated with the 9×9 (full lines) and 10×10 (broken lines) superstructures, for different numbers of Cu vacancies per unit cell ($n_v = 0$, 4, and 5).

In order to obtain an atomic-scale insight into the stress distribution in the system, in Figs. 3(a) and 3(b) we show the maps of local pressure[32–34] undergone by the atoms of the first two planes: the adsorbate Ag plane and the first Cu substrate layer.[23] A striking feature is the almost complete reversal between the images of Ag and Cu layers. More precisely, all the Ag atoms undergo a tensile pressure, the most tensile ones being concentrated in localized regions with rounded shapes. Conversely, the Cu plane presents both compressive and tensile regions, the sites in maximum compression lying just below the Ag ones presenting the maximum tensile stress. The underlying planes present a similar compression which is completely damped beyond the tenth layer only. This implies that the most strained regions are made up of columns of atoms ended by the most tensile sites of the Ag adlayer. Let us recall that these Ag tensile sites are those placed in on-top or close to on-top positions with respect to the underlying Cu atoms, corresponding locally to a {**A**(Ag)-**A**(Cu)-**B**(Cu)-**C**(Cu)-**A**(Cu)-$\cdots$} stacking, as described schematically in Fig. 4. Surprisingly the Ag sites with the highest elevation are the hexagonal-close-packed (hcp) ones, corresponding to the local {**B**(Ag)-**A**(Cu)-

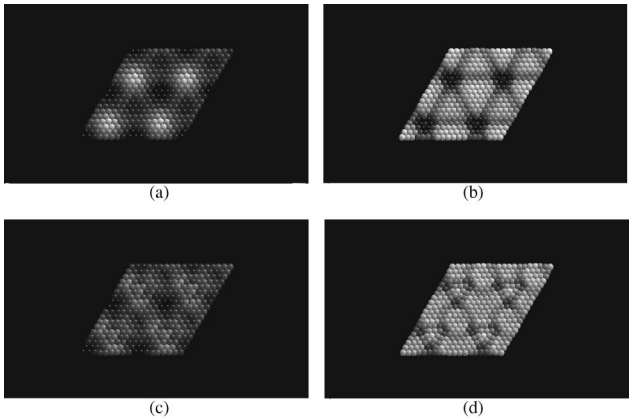

FIG. 3. Local pressure maps in the Ag [(a) and (c)] and Cu [(b) and (d)] layers for the 10×10 superstructure, without [(a) and (b)] and with five Cu vacancies [(c) and (d)]. The gray scale is chosen such as the white (black) atoms are the most tensile (compressed) ones with the following extreme values: In the Ag layer, $P_{\mathrm{min}} = -88$ kbar, and $P_{\mathrm{max}} = +19$ kbar; and in the Cu layer $P_{\mathrm{min}} = -77$ kbar, and $P_{\mathrm{max}} = +84$ kbar.

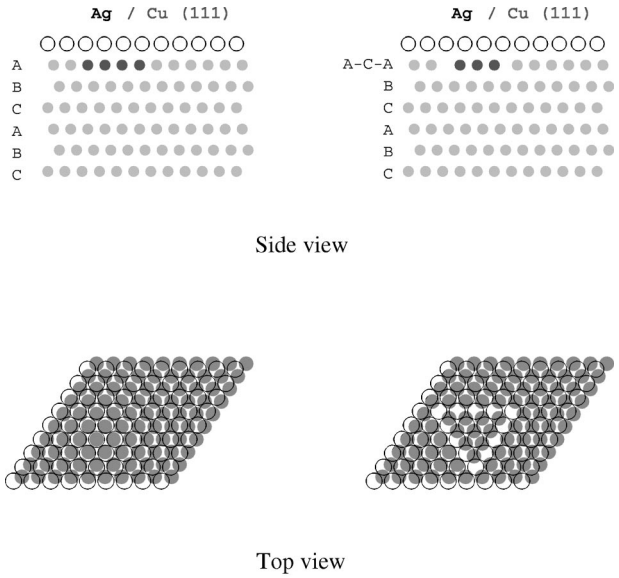

FIG. 4. Schematics of the stacking fault, which allows one to avoid unfavorable on-top positions (left-hand side), by the introduction of a partial dislocation loop (right-hand side). The Ag (Cu) atoms are represented by empty (gray) circles. Upper side: schematic profile view. The darker circles label the Cu atoms initially in ''unfavorable'' positions. Lower side: top view of the first two layers (Ag and Cu).

B(Cu)-**C**(Cu)-**A**(Cu)-$\cdots$} stacking, whereas the Ag atoms placed in the on-top position are those with the lowest elevation, this result also being recovered by EAM simulation.[35]

A way to relax partially the interfacial stress should be to avoid such unfavorable positions by removing atoms from regions where they are the less coordinated, either from the Ag adlayer or from the first Cu substrate plane. Another way is to create a local stacking fault on one of the first two planes to eliminate the on-top positions, either in the Ag plane or the Cu plane. In this latter case the stacking {**A**(Ag)-**A**(Cu)-**B**(Cu)-**C**(Cu)-**A**(Cu)-$\cdots$} is replaced by {**A**(Ag)-**C**(Cu)-**B**(Cu)-**C**(Cu)-**A**(Cu)-$\cdots$} (see Fig. 4). We will see in the following sections that this localized stacking fault, surrounded by partial dislocation loops, also requires the formation of Ag or Cu vacancies. This means that the two processes of interfacial stress relaxation (point defects and dislocation loops) are strongly connected.

B. Creation of vacancies in the Ag adlayer

As mentioned above, it is tempting to relax the stress by introducing vacancies within the Ag adlayer. This is what we have done by removing successively the Ag atoms in the on-top or close to on-top position for the 10×10 periodicity. The perfectly on-top position is unique, as can be seen in Fig. 4. Therefore, there is no ambiguity for removing a single vacancy. The choice is more puzzling in what concerns the following removals, since the structure is symmetric around the perfect on-top position, presenting six less coordinated equivalent sites. Then, instead of squeezing out one over these six atoms, we prefer to remove them along a close-packed row near the on-top atom, in order to let the others relax without constraint. As can be seen in Fig. 5, the introduction of Ag vacancies leads to a continuous increase of the

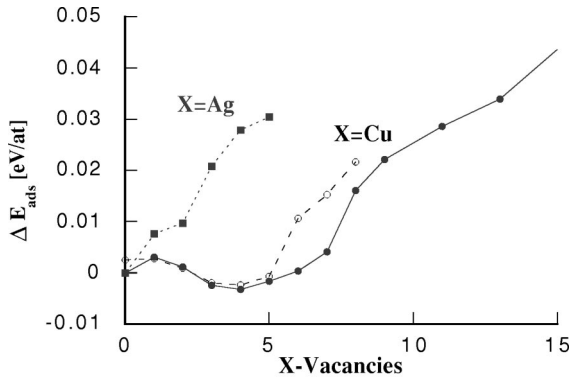

FIG. 5. Variation of the adsorption energy in eV/at with respect to the one of the 10×10 superstructure without vacancies, as a function of the number of either Ag vacancies in the 10×10 superstructure (dotted line), or Cu vacancies in the 10×10 (full line) and 9×9 (broken line) superstructures.

adsorption energy whatever their concentration. This means that the system ''prefers'' to accommodate the stress induced by the on-top atoms by allowing a long-range corrugation into the substrate rather than to lower the atomic density in the Ag adlayer. Thus the triangular shaped regions observed by STM cannot be attributed to Ag vacancies.

C. Creation of vacancies in the first Cu substrate layer

Let us now study the effect of introducing n_v Cu vacancies per unit cell in the first substrate layer. This means that we have to locate the Cu atoms which have been removed elsewhere. The choice of this location is far for being simple. Indeed, two main situations can be encountered depending on that one favours either thermodynamical or kinetical arguments.

(i) In the former case, i.e., from a thermodynamical point of view, the stablest situation is to locate the removed atoms at some substrate step edges.

(ii) In the latter case, i.e., from a kinetical point of view, a possible transient state could be found at least for a system presenting a wide range of miscibility in the bulk phase diagram, by relocating the removed substrate atoms within the deposit adlayer, forming a two-dimensional dilute surface alloy.

Here, consistently with our aim to find the stablest structure at equilibrium, we have chosen to follow the thermodynamical prescription, i.e., to locate the removed atoms at kinks. This is the most natural way as the kinetic solution does not apply to our case since the miscibility between Ag and Cu is very low in the bulk.

Two extreme ways exist to introduce n_v Cu vacancies, either in a nonlocalized way by suppressing one Cu atom in each of n_v close-packed rows before shifting continuously the remaining Cu atoms along these rows, or in a more localized way by removing the Cu atoms which are in the close vicinity of the perfectly on-top Ag atom (in practice, we remove these Cu atoms along a close-packed row, passing through this on-top position). For the first case (continuous shift of the Cu atoms), the relaxation leads to the superstructure shown in Fig. 1(c) for the 10×10 unit cell with four and five vacancies. We can observe triangular-shaped regions with one or three protruding atoms in the center, in excellent

agreement with STM images. In the bottom of Fig. 4, we show a schematics of the final configurations of the first two planes (the Ag adlayer plane and the first Cu substrate one) for the 10×10 unit cell with five vacancies, initially nonlocalized.

Let us remark on the efficiency of the relaxation algorithm, which leads to a localization of the shifted Cu atoms, the n_v vacancies themselves being distributed along a triangular boundary. In fact, the same triangular structure is obtained if one introduces the vacancies in a more localized way, following the second proposed procedure. This confirms that this structure is the stablest one and not a metastable solution, since it is obtained whatever the initial configuration. It is worth noting that such a configuration has been already obtained for small vacancy clusters in bulk fcc metals.[36,37] The Cu atoms inside the triangle are now in a hcp position relatively to the Cu substrate. This allows the Ag atoms, which were previously in on-top or close to on-top positions, to be in ternary hollow positions. Moreover the Ag atoms along the triangle edges are in a fourfold position, and the triangular corner Ag atoms are in a fivefold position, which leads to more favorable Cu-Ag bonding.

The minimum values of the adsorption energy are found for $3\leqslant n_v\leqslant5$, the absolute minimum being reached for four vacancies for the 10×10 structure. The obtained value, both for the 9×9 and 10×10 superstructures, is very close to the Moiré structure one (i.e., without Cu vacancies), since it is lower by only 0.004 eV/at. This is consistent with the observation of the two structures, depending on the temperature.[19]

Let us conclude this section by noting that the Cu vacancy formation energy becomes negative for $3\leqslant n_v\leqslant5$. This is very similar to the stress relaxation process predicted for clusters of icosahedral structure.[38] In this case, the existence of a constitutive central vacancy is shown to be the most efficient way to relax internal stress due to the icosahedral stacking.

For the present case, the low (and even negative) value of the vacancy formation energy on given sites of the first Cu substrate plane can shed some light on the atomic mechanism responsible for the superstructure. In fact it is well known that the superficial (ad)vacancy concentration is higher than the bulk one. This is a consequence of the lower vacancy formation energy at the surface, which is itself mainly due to the smaller number of broken bonds necessary to create an advacancy. As the surface contains a lot of sources and sinks of point defects, the superficial vacancy concentration reaches (or retains) its equilibrium value very easily. Since a part of these superficial vacancies must segregate in the favorable zones of the first substrate plane described above, we can expect rapid exchanges between advacancies and the concerned Cu atoms of this plane. However, a detailed calculation of the various migration barriers is necessary before concluding on the preponderance of a given mechanism.

D. Introduction of partial dislocation loops in the first Cu substrate layer

We just have seen that the formation of four or five vacancies per unit cell in the first substrate plane, for the 9×9 or 10×10 superstructures, allows us to avoid the on-top position of some Ag atoms. The triangular shape is in fact a localized region where the stacking {**A**(Ag)-**A**(Cu)-**B**(Cu)-**C**(Cu)-**A**(Cu)-$\cdots$} is replaced by {**A**(Ag)-**C**(Cu)-**B**(Cu)-**C**(Cu)-**A**(Cu)-$\cdots$}, leading to a stacking fault in the first substrate plane (see Fig. 4). It is well known that a localized stacking fault can be formed in the bulk by dissociation of a perfect dislocation into Shockley partials or by Frank dislocations, for instance produced by aggregation of vacancies.[39,40] A famous example is the stacking-fault tetrahedra observed in quenched gold,[41] silver, and also nickel-cobalt alloys.[40] However, this peculiar geometry is a three-dimensional (3D) one. Thus one can ask about the relation between the extension of the stacking fault and the number of point defects necessary to its creation in the present quasi-2D geometry.

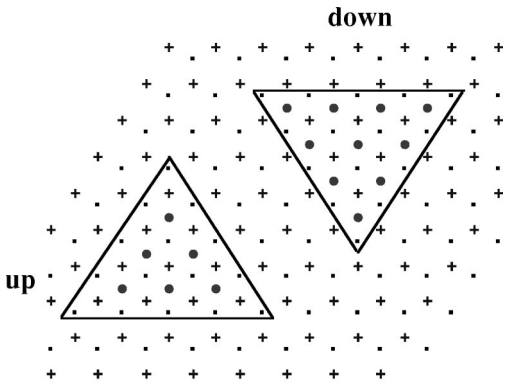

FIG. 6. Vacancy condensation in the A layer of a fcc $\ldots C/A/B/C/\ldots$ stacking. The dots are used for atoms of type A, the full circles for those of type C, and the crosses for those of type B atoms. Only the triangular loops of 15 vacancies in the A layer are shown. The other loop sizes (3, 6, 10, and 21) indicated in Table I, are obtained in a similar way.

To answer this question, let us consider Frank dislocations running along $\langle1\bar{1}0\rangle$-type directions (i.e., a triangular loop) in the first (111) surface layer of a pure semi-infinite Cu crystal with the stacking C(surface)-A-B-C-A $\ldots$. This is obtained by vacancy condensation (see Fig. 6) in the first underlayer (A). However, as can be seen in this figure, depending on whether the orientation of the loop is down ($\bigtriangledown$) or up ($\bigtriangleup$), the number of C sites is greater or smaller than the number of B sites inside the triangular loop. As a consequence, for the down orientation, we can expect a giant relaxation of the surface atoms, those above the triangular loop of vacancies going into the C sites inside the triangular loop.

TABLE I. Relation between the size of the Frank loop (in number of vacancies, n_{Frank}); the faulted Cu triangle (in number of Cu atoms, n_{Cu}); the number of Cu vacancies per unit cell, n_v; the length of the Ag triangle edges (in number of Ag atoms, $\mathrm{Ag_{edge}}$); and the number of protruding Ag atoms, $\mathrm{Ag_{protruding}}$.

n_{Frank}	n_{Cu}	n_v	$\mathrm{Ag_{edge}}$	$\mathrm{Ag_{protruding}}$
3	1	2	2	0
6	3	3	3	0
10	6	4	4	1
15	10	5	5	3
21	15	6	6	6

TABLE II. Corrugation of the Ag atoms occupying the different sites above the Cu stacking fault. The experimental data (Ref. 20) are given with an uncertainty of ± 0.05 Å. The theoretical values are averaged on the various sites, which leads to a dispersion of about ± 0.10 Å.

	10×10 $n_v=5$	10×10 $n_v=4$	9×9 $n_v=5$	9×9 $n_v=4$	Experiment
vertex	−0.54 Å	−0.65 Å	−0.32 Å	−0.55 Å	−0.20 Å
edge	−0.27 Å	−0.36 Å	−0.31 Å	−0.32 Å	−0.20 Å
center	−0.02 Å	−0.16 Å	−0.00 Å	−0.13 Å	−0.00 Å

Let us recall that such phenomena are obtained for small vacancies clusters in fcc bulk crystal.[36,37] If we now remove the remaining surface atoms, the *A* plane with its triangular stacking fault is correctly prepared to become the first substrate layer recovered by the Ag adlayer. In Table I, we give the relation between the number of vacancies forming the initial Frank loop, the number of effective Cu vacancies and Cu atoms in the faulted triangle in the first underlayer after the giant relaxation of the surface atoms, and the number of Ag atoms in the triangle in the adlayer plane. For this latter quantity, we distinguish the atoms above the faulted Cu triangle (which are the protruding atoms) from the Ag atoms of the triangle edges.

With this construction, we see that the four (five) Cu vacancies case corresponds precisely to Ag triangles with edges four (five) atoms in length and one (three) protruding atom. Moreover, it unifies the description of the superstructure in terms of point defects or dislocation loops in the first underlayer. Finally, it explains the orientation of the triangle (up or down). Thus it allows us to conclude that a step does not change the orientation of the triangles, whereas the presence of a buried twin parallel to the surface must change it.

IV. COMPARISON WITH EXPERIMENTS AND LOCAL ANALYSIS

A. Comparison with experiments

Let us now compare the atomic structure of the Ag layer with the STM image of Fig. 1(b).[20] In Fig. 1(c) we show the 10×10 relaxed structure corresponding to the two most stable situations, i.e., with triangles edged, respectively, by four and five atoms (obtained by introducing four and five Cu vacancies, respectively, per unit cell in the first substrate layer). One can see that the agreement with STM images is strongly improved with respect to the configuration without vacancies [the Moiré structure, Fig. 1(a)]. Indeed, the hollowed regions associated with the tensile areas of the Moiré structure have been replaced by deep triangular-shaped regions, edged by four or five atoms, with one or three protruding atoms in the center. The same morphology with triangles and protruding atoms is observed equally for the 9×9 structure.

Let us go into more detail in the description of these triangles. In Table II, we can see that the elevation strongly differs from one site (vertex, edge, and center) to the other. In particular, the vertices are found deeper than the edge atoms, except for the five-atom-edged triangles in the 9×9 structure. This is in quite good agreement with the experimental line scans, giving the corrugation amplitude along a direction parallel to one triangle edge.[20] Moreover the corrugation is more pronounced for the 10×10 structure than for the 9×9 one. Finally, it is worth noticing that a mixing of 9×9 and 10×10 superstructures could be consistent with the periodicity given by SXRD experiments, namely, 9.43×9.43.[20] Moreover, preliminary simulations of the in-plane SXRD reflections using our stablest structures as input reveal a very good agreement.

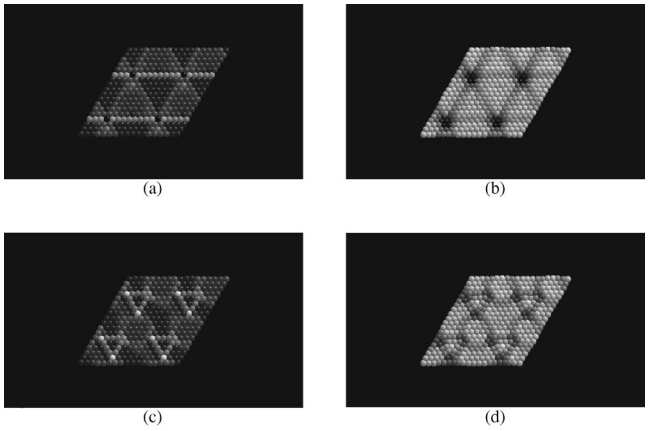

FIG. 7. Local energy maps in the Ag [(a) and (c)] and Cu [(b) and (d)] layers for the 10×10 superstructure, without [(a) and (b)] and with five Cu vacancies [(c) and (d)]. The gray scale is chosen such that the white (black) atoms are the most favorable (unfavorable) ones with the following extreme values: in the Ag layer, $E_{\min}=-2.91$ eV/at and $E_{\max}=-2.73$ eV/at; and in the Cu layer, $E_{\min}=-3.42$ eV/at and $E_{\max}=-3.24$ eV/at.

Let us mention that similar dislocation loops in the first substrate layer have also been observed in the Au/Ni system.[42] However, in that case, the reconstruction of the first Ni substrate layer was associated with the formation of a dilute Au(Ni) surface alloy, the STM images showing evidence of Ni atoms incorporated in the Au overlayer. Here the STM images presented in Fig. 1(b) for the Ag/Cu(111) system do not indicate a similar incorporation of Cu atoms in the Ag adlayer, even though one has to be cautious before drawing definite conclusions since the present images both present smaller areas and have lower resolution than those obtained for Au/Ni.[42] Our study shows that this mechanism for epitaxial stress relaxation can be efficient without resorting to surface alloy formation.

B. Local analysis

A main characteristic of the triangular structure is to exhibit Ag atoms occupying ternary sites instead of the unfavorable on-top sites present in the Moiré structure. Actually the triangular region is essentially made of a triangular stacking fault surrounded by a partial dislocation loop. Above this loop, which forms a channel, the Ag adatoms can occupy positions in which they are bounded to four neighbors, or even five neighbors in the corners. Such an evolution toward a more close-packed structure allows one to gain sufficient energy to compensate for the stacking fault energy and the vacancy formation energy. This can be seen in Fig. 7, in which we plot the maps indicating the local energy in each site for the first two planes (the Ag adlayer and the first Cu

underlayer) before and after the introduction of Cu vacancies. Indeed, in the Ag adlayer the very unfavorable on-top sites are now avoided, whereas new favorable sites appear, corresponding to the fivefold and fourfold positions. The situation is more complex in the Cu layer, but it can be seen that the most unfavorable sites have now been suppressed by the introduction of vacancies, which is the signature of a more general release of the stress.

The pressure map associated with the triangular structure confirms that the introduction of vacancies is an efficient way to relax the stress. This is shown in Figs. 3(c) and 3(d). As a main effect the compressive stress is reduced and distributed more uniformly in the first Cu layer. At the atomic level, this stress relief is followed by a significant change in the corrugation profile of the Cu layers. As can be seen in Fig. 2, the corrugation is more rapidly damped and its amplitude widely lowered, both for the 10×10 and 9×9 structures. The situation is slightly different for the Ag layer. Its corrugation is unchanged for the 10×10 periodicity, whereas a significant lowering is observed for the 9×9 superstructure, at least for the case of four vacancies per unit cell .

V. CONCLUSION AND PERSPECTIVES

In this paper, we have studied different ways to relax the interfacial stress due to a strong size mismatch in heteroepitaxy for the Ag/Cu(111) system. Whereas the general way to release the stress is to consider different configurations for the deposited element (introduction of dislocations in the adlayer or continuous matching of the deposit relatively to the substrate), here we show that the adlayer reconstruction can be made more efficient by coupling it to a reconstruction of the first substrate layer. More precisely, introducing a few Cu vacancies collapsing in a partial dislocation loop allows us to avoid the very unfavorable on-top positions by creating a stacking fault under the Ag adsorbate layer. The introduction of the dislocation loop in the substrate has two main consequences compared to the previously proposed structure without Cu vacancies. First, it strongly reduces the extension toward the substrate of the perturbation, characterized by the corrugation and the stress induced by the adlayer. Second, the calculated morphology is now in almost perfect agreement with the STM images. Let us note that such a dislocation loop in the first substrate layer is stabilized without resorting to any Cu-Ag mixing in the deposited adlayer, and then without formation of a dilute two-dimensional surface alloy.

We now plan to develop this work along two directions. First of all, from an experimental point of view, detailed SXRD data are now available which could be compared with the lines simulated from the triangular structure. The analysis is currently in progress.[43] Then, from a theoretical point of view, it should be interesting to identify the atomic mechanisms involved in the creation of the stacking fault. In particular, this implies quantifing the corresponding activation barriers. Moreover, one can wonder about the influence of this superstructure on the dissolution process of 1-ML Ag/Cu(111) on the one hand, and on the kinetics of segregation in Cu(Ag)(111) on the other hand. From this point of view the preliminary STM data of the first dissolution stages are very promising, and calculations are in progress thereupon.

ACKNOWLEDGMENTS

The authors are indebted to D. Rodney and N.V. Doan for giving them useful information concerning their work about vacancy clusters in fcc metals. They are also very grateful to F. Besenbacher and J.K. Norskov for useful discussions about their surface alloy studies.

*The CRMC2 is also associated to the Universities of Aix-Marseille II and III.

[1] J. W. Matthews, in *Epitaxial Growth*, edited by J. W. Matthews (Academic, New York, 1975), pt. 1, p. 559.
[2] J. H. van der Merwe, in *Chemistry and Physics of Solid Surfaces*, edited by R. Vanselow and R. Howe (Springer, Berlin, 1984), p. 365.
[3] B. W. Dodson, in *Heteroepitaxy on Silicon: Fundamentals, Structures, and Devices*, edited by H. K. Choi, R. Hull, H. Ishiuana, and R. J. Nemanich, MRS Symposium Proceedings No. 116 (Materials Research Society, Pittsburgh, 1980), p. 491.
[4] M. H. Grabow and G. H. Gilmer, in *Initial Stages of Epitaxial Growth*, edited by R. Hull, J. M. Gibson, and O. A. Smith, MRS Symposia Proceedings No. 94 (Materials Research Society, Pittsburgh, 1987), p. 15.
[5] J. H. van der Merwe, D. L. Tönsing, and P. M. Stoop, Surf. Sci. **312**, 387 (1994).
[6] M. Henzler, Surf. Sci. **357-358**, 809 (1996).
[7] S. Tan, A. Ghazali, and J. C. S. Lévy, Surf. Sci. **369**, 360 (1996).
[8] E. Bauer, Surf. Sci. **7**, 351 (1967).
[9] K. A. R. Mitchell, D. P. Woodruff, and G. W. Vernon, Surf. Sci. **46**, 418 (1974).
[10] E. Bauer, Appl. Surf. Sci. **11-12**, 479 (1982).
[11] P. A. Huttunen, J. Mákinen, and A. Vehanen, Phys. Rev. B **41**, 8062 (1990).
[12] P. A. Huttunen and A. Vehanen, Phys. Rev. B **42**, 11 570 (1990).
[13] Y. Liu and P. Wynblatt, Surf. Sci. **240**, 245 (1990).
[14] J. Eugène, B. Aufray, and F. Cabané, Surf. Sci. **241**, 1 (1991).
[15] Y. Liu and P. Wynblatt, Surf. Sci. **241**, L21 (1991).
[16] Y. Liu and P. Wynblatt, Surf. Sci. **310**, 27 (1994).
[17] W. E. MacMahon, E. S. Hirschorn, and T. C. Chiang, Surf. Sci. **279**, L231 (1992).
[18] S. Mroz and M. Nowicki, Surf. Sci. **297**, 66 (1993).
[19] F. Besenbacher, L. Pleth Nielsen, and P. T. Sprunger, in *The Chemical Physics of Solid Surfaces and Heterogeneous Catalysis*, edited by D. A. King and D. P. Woodruff (Elsevier, Amsterdam, 1997), Vol. 8, Chap. 10.
[20] B. Aufray, M. Göthelid, J.-M. Gay, C. Mottet, E. Landemark, G. Falkenberg, L. Lottermoser, L. Seehofer, and R. L. Johnson, Microsc. Microanal. Microstruct. **8**, 167 (1997).
[21] G. Tréglia, B. Legrand, J. Eugène, B. Aufray, and F. Cabané, Phys. Rev. B **44**, 5842 (1991).
[22] C. Mottet, G. Tréglia, and B. Legrand, Phys. Rev. B **46**, 16 018 (1992).
[23] C. Mottet, G. Tréglia, and B. Legrand, Surf. Sci. **287-288**, 476 (1993).
[24] V. Rosato, M. Guillopé, and B. Legrand, Philos. Mag. A **59**, 321 (1989).
[25] R. Hultgren, P. D. Desay, D. T. Hawkins, M. Gleiser, K. K.

Kelley, and D. D. Wagman, *Selected Values of Thermodynamic Properties of the Elements* (American Society of Metals, Ohio, 1973).
[26] M. S. Daw and M. I. Baskes, Phys. Rev. B **29**, 6443 (1984).
[27] P. Stoltze, J. Phys.: Condens. Matter **6**, 9495 (1994).
[28] M. W. Finnis and J. E. Sinclair, Philos. Mag. A **50**, 45 (1984).
[29] F. Ercolessi, E. Tosatti, and M. Parrinello, Phys. Rev. Lett. **57**, 719 (1986).
[30] G. Tréglia, B. Legrand, and F. Ducastelle, Europhys. Lett. **7**, 575 (1988).
[31] C. H. Bennett, in *Diffusion in Solids, Recent Developments*, edited by A. S. Nowick and J. J. Burton (Academic, New York, 1975), p. 73.
[32] D. J. Srolovitz, K. Maeda, V. Vitek, and T. Egami, Philos. Mag. A **44**, 847 (1981).
[33] T. Egami and V. Vitek, J. Non-Cryst. Solids **61-62**, 499 (1984).
[34] V. Vitek and T. Egami, Phys. Status Solidi B **144**, 145 (1987).
[35] S. M. Foiles, Surf. Sci. **292**, 5 (1993).
[36] N. V. Doan, in *Point Defects and Defect Interactions in Metals*, edited by J. Takamura, M. Doyama, and M. Kiritani (University of Tokyo Press, Tokyo, 1982), p. 722.
[37] A. G. Crocker, M. Doneghan, and K.W. Ingle, Philos. Mag. A **41**, 21 (1980).
[38] C. Mottet, G. Tréglia, and B. Legrand, Surf. Sci. **383**, L719 (1997).
[39] J. Friedel, *Dislocations* (Pergamon, Oxford, 1964).
[40] J. P. Hirth and J. Lothe, *Theory of Dislocations* (Krieger, Malabar, FL, 1992), p. 331.
[41] J. Silcox and P. B. Hirsch, Philos. Mag. **4**, 72 (1959).
[42] J. Jacobsen, L. Pleth Nielsen, F. Besenbacher, I. Stensgaard, E. Lægsgaard, T. Rasmussen, K. W. Jacobsen, and J. K. Norskov, Phys. Rev. Lett. **75**, 489 (1995).
[43] J.-M. Gay, I. Meunier, G. Tréglia, and B. Aufray (unpublished).